Net-Zero Energy Dual-Functional Radar-Communication Systems

Iman Valiulahi, Christos Masouros, *Senior Member,* IEEE, Abdelhamid Salem, *Member,* IEEE

***Abstract*—This paper proposes beamforming designs for net-zero energy multi-input multi-output (MIMO) dual-functional radar-communication (DFRC) systems that are powered through energy harvesting (EH) resources and aim to operate autonomously without access to the power grid. We propose a weighted optimization problem to jointly maximize the radar mutual information and minimum quality of service (QoS) requested by communication users subject to energy balancing constraints. The proposed problem is not convex, hence it is tough to solve. We exploit semidefinite relaxation (SDR) and first-order Taylor expansion techniques to relax its non-convexity issues. We then propose an iterative algorithm to obtain the beamforming matrices for the reference scenario when full channel state information (CSI) and energy arrival information (EAI) are available. For the single-target scenario, we show that the proposed optimization contains rank-one solutions. For the multiple targets scenario, by adding auxiliary optimization variables, we show that rank-one matrices can be achieved from the optimal solutions of the proposed optimization. We then propose a robust optimization for the case where only imperfect CSI and EAI are assumed to be known. Finally, numerical simulations show that the proposed DFRC designs are convergent and obtain a graceful trade-off between the radar and communication performances.**

***Index Terms*—Energy harvesting, dual-functional radar-communication systems, mutual information, and semidefinite relaxation.**

I. Introduction

To enhance spectrum, energy, and hardware efficiency in radar and communication systems, recently, there has been a growing interest in exploiting multiple-input multiple-output (MIMO) dual-functional radar-communication (DFRC) systems where a single access point (AP) accommodates both radar and communication tasks simultaneously [1]–[13]. Despite the above benefits, the current state-of-the-art DFRC systems have several key challenges that need to be addressed. First, the joint beamforming design that can sense targets and deliver communication messages is non-trivial. Second, wireless transmitters including multiple antennas and their radio frequency (RF) chains require a considerable amount of energy [14], [15], which makes the development of energy-efficient designs necessary.

In terms of DFRC signaling design, three major categories of approaches can be defined in the literature. Firstly, radar-centric designs employ typical radar waveforms and encode data signals through index modulation techniques [1]. For example, in [2], by exploiting the inherent spatial and spectral randomness of the carrier agile phased array radar (CAESAR), the authors studied a DFRC-AP that conveys digital messages in the form of index modulation. Secondly, communication-centric designs where existing communication signals such as orthogonal frequency division multiplexing (OFDM) [3] or standards relevant wireless local area network (WLAN) signals [4] were used as reference signals to detect targets. Thirdly, and most relevant to our paper, involve designing waveforms from the start in order to simultaneously convey communication messages and detect radar targets [5]–[8]. In [5], the authors obtained a power-efficient DFRC system by exploiting the constructive multi users interference. For a certain level of signal-to-noise-plus-interference ratio (SINR) of communication users, a co-design of radar waveform and communication transmit weights that minimizes Cramér-Rao Bound (CRB) of radar was proposed in [6]. Reference [7] aimed to maximize the radar performance while guaranteeing the SINR at each communication user. In [8], the authors proposed a non-convex optimization that minimizes the CRB subject to the SINR and antenna selection constraints. In [16], a novel bandwidth allocation strategy is proposed in order to optimize the weighted average range resolution for sensing, and guarantee the sum-rate among communication users.

To address the second issue of energy efficiency, a proliferation of studies in the communication-only literature has focused on hardware informed design through few-RF chain implementations [17], few-bit DAC solutions [18], antenna selection [19] among other methodologies. Most recently, net-zero operation has been brought to the forefront of research in order to design systems that operate by balancing the energy consumed with the energy harvested and the energy stored. Towards net-zero energy APs, one can deploy energy harvesting (EH) devices such as wind turbines and solar panels at the AP to reduce the energy consumption costs, and there are a number of studies in the communication-only literature towards this end [20]–[25]. References [20], [21], and [22] studied multiple access, broadcast, and relay channels for EH APs, respectively. A transmission time minimization for an EH AP with a finite battery capacity was investigated in [23]. For OFDM signaling, in [24], power allocation policies were proposed using the binary user scheduling method. The authors of [25] studied joint power scheduling and antenna selection using zero-forcing (ZF) transmission method for the multi-antenna EH APs. However, all the mentioned works considered energy balancing constraints for the communication-only APs and there is still a lack of studying zero-net energy DFRC-APs. Accordingly, the main goal of this paper is to study the signaling and energy balancing design for a net-zero energy DFRC-AP, that is equipped with an EH device with a limited battery capacity that can collect energy from the environment.

The authors are with the Department of Electronic and Electrical Engineering, University College London, London WC1E 7JE, U.K. (e-mails: i.valiulahi@ucl.ac.uk; c.masouros@ucl.ac.uk)

This article has been accepted for publication in IEEE Transactions on Green Communications and Networking. This is the author's version which has not been fully edited and content may change prior to final publication. Citation information: DOI 10.1109/TGCN.2023.3236029

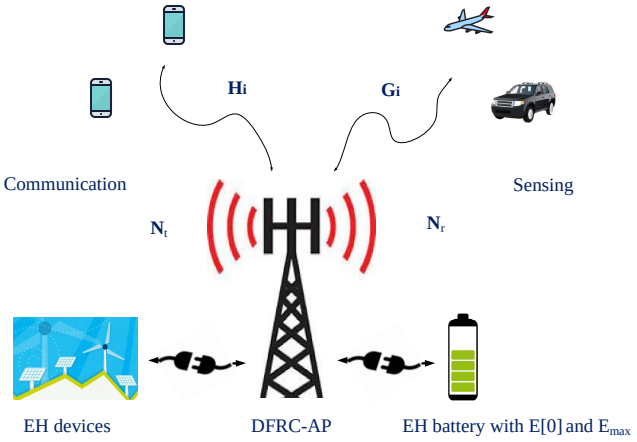

Fig. 1: A net-zero energy DFRC system.

Moving from the communication-only studies to the DFRC design requires integrating radar performance metrics into the communication system design. The MIMO radar literature is abundant with several performance metrics such as CRB [26], SINR [27], [28], and minimum mean-square error (MMSE) [29], [30]. However, the information-theoretic performance metrics have shown a significant superiority [31]–[34]. For instance in [31], the authors proved that maximizing the mutual information between the target ensemble and reflected signal from the targets can improve the radar performance in terms of target estimation, classification, and identification. The authors in [32] showed that for the linear-Gaussian channel, mutual information maximization and MMSE minimization have the same optimal MIMO waveforms. Moreover, for the uncorrelated targets in the MIMO radar, the authors in [33] proved that maximization of mutual information can obtain the Chernoff bound. Also, from the communication perspective, providing the minimum quality of service (QoS) requested by the users is a promising communication performance metric, which has been widely used in different communication system problems [35].

Existing works in the DFRC literature mainly optimize the radar and communication performance metrics separately and there is still a lack of joint radar and communication performance metrics optimization [1]–[8]. Building on the mentioned benefits of mutual information maximization as the radar performance metric, in this paper, we propose a novel optimization that jointly maximizes both the radar mutual information and minimum communication QoS. We assume that the consumed energy can be provided by the EH sources, which is the first time studied in the DFRC literature. Hence, the proposed optimization problem is required to satisfy two inherent energy conditions, casualty and battery overflow constraints [20]–[25]. The first ensures that no more energy than the that available at any given time can be consumed [24], [25] and the second one considers the energy storage capacity to avoid the EH battery to overflow [24], [25]. The main contributions of this work are summarized as follows.

- To obtain a reference performance benchmark, we first assume that full channel state information (CSI) and energy arrival information (EAI) are available at the DFRC-AP. Since the proposed optimization problem is not convex, we exploit semidefinite relaxation (SDR) and first-order Taylor expansion techniques to relax the non-convexity of the proposed problem.
- We then propose an iterative algorithm to tighten the approximation bound of Taylor expansions. Our contribution further involves a proof of the convergence of the proposed algorithm.
- In this paper, we consider two different target models, single-target and multiple targets scenarios. For the single-target case, we show that the proposed optimization can obtain rank-one solutions. For the multiple targets scenario, we add auxiliary variables to the proposed optimization and show that one can always obtain rank-one beamforming matrices from the optimal solutions of the proposed optimization.
- To provide a practical resource allocation, we study a robust optimization for the case where only imperfect CSI and EAI are known at the DFRC-AP.
- We perform numerical simulations to evaluate the performance of the proposed DFRC designs. They demonstrate that through the proposed weighted optimization problem, one can obtain a graceful trade-off between the radar and communication performances. They show that the proposed DFRC designs quickly converge. Also, they illustrate that the performance of the robust designs (RD)s is comparable to the full CSI and EAI scenario and depends on the accuracy of prior knowledge regarding CSI and EAI.

The paper is organized as follows: The system model and problem formulation are presented in Section II. Section III is devoted to the full CSI and EAI designs. The robust optimization is given in Section IV. Numerical experiments are presented in Section V. Section VI concludes the paper.

Throughout the paper, scalars, vectors, and matrices are denoted by lowercase, lowercase boldface, and uppercase boldface letters, respectively. The operators $(\cdot)^T$, $(\cdot)^H$, and $\mathbb{E}\{\cdot\}$ represent the transpose, hermitian of a matrix, and the expectation of a random process, respectively. We use $\boldsymbol{I}_N$ to show the identity matrix with the size $N \times N$. The absolute value and norm two are denoted by $|\cdot|$ and $\|\cdot\|$, respectively. The determinate of a matrix is shown by $\det(\cdot)$. We use the symbol $\otimes$ to denote the Kronecker product.

II. System Model and Problem Formulation

We consider an EH MIMO DFRC system, as shown in Fig. 1, with a DFRC-AP with N_t and N_r transmitting and receiving antennas, respectively, M users with a single antenna each, and K targets. Without loss of generality, we assume that $N_t = N_r$ and $M + K \leq N_t$. The AP is equipped with an EH device that has a battery with the maximum capacity $E_{\max}$. The harvested energy can be stored in the battery or consumed for transmission. The EH DFRC-AP accommodates both radar and communication tasks simultaneously. Indeed, it communicates with the M users and senses K targets with a single transmission. Suppose that during the transmission

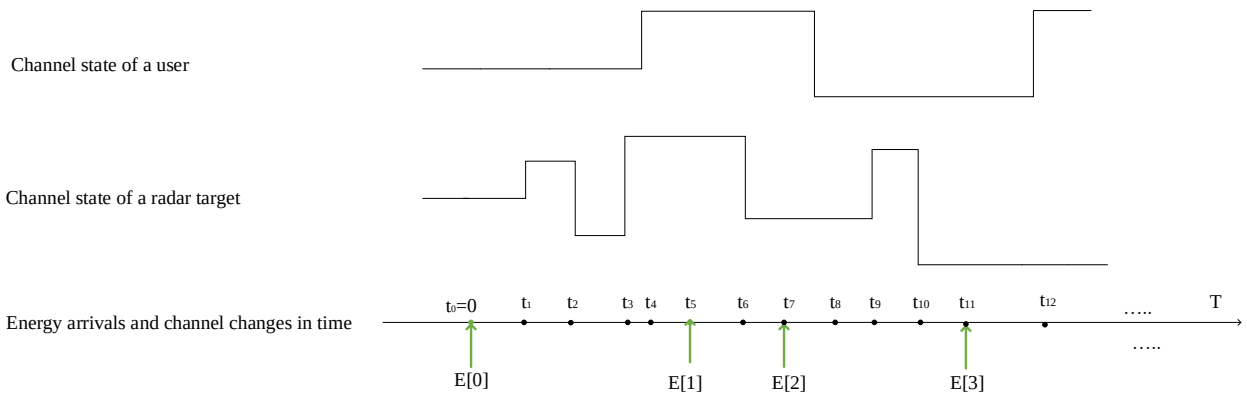

Fig. 2: An illustration of the events over the transmission interval, $[0, T)$.

interval, $[0, T)$, energies arrive L_e times, following a Poisson process with rate λ_e. The energy arrival values also follow a uniform distribution with parameters $e_{\min}$ and $e_{\max}$, i.e., $E[i] \backsim U(e_{\min}, e_{\max})$ for $i \in \{1, \cdots, L_e\}$. We also assume that the stored energy in the battery at the beginning of the operation is $E[0]$. Following [24], [25], we employ a full-duplex battery that can be charged or discharged at the same time. For the communication channel, we consider a block fading model where the channel states are constant during each block and change over the consecutive blocks independently. Moreover, we assume that channel states change L_c times during the transmission interval, following a Poisson process with rate λ_c. For notional convenience, let us assume that all the communication users have the same coherence time, though our model can be readily generalized to the case where the users have different coherence times at the cost of more variables. Similar to the communication channel, for the radar two-way channel, we assume that the channel states change L_r times with a Poisson process with rate λ_r. This can be translated to moving targets or changes in the environment. It is also assumed that all the targets have the same coherence time for the sake of notation simplicity. Fig. 2 illustrates an example of these changes.

To represent energy arrivals, communication, and radar changes in our proposed DFRC designs, we assume that the time indices of all three changes are comparable. We define any change of communication, radar channel states, or energy arrivals as an *event*. Then, the time interval between two consecutive events is defined as an *epoch*. The number of events during the transmission time is obtained as $L_E = L_e + L_c + L_r$. Consequently, the epoch length can be given by $\ell_i = t_i - t_{i-1},\ \forall i \in \{1, 2, \cdots, L_E + 1\}$ in which t_i is the associated time with the i-th epoch. It is worth noting that $\ell_1 = t_1$, where t_1 is the corresponding time with the first event, as $t_0 = 0$. Moreover, $\ell_{L_E+1} = T - t_{L_E}$ in which t_{L_E} and T_{L_E+1} is the corresponding time with the last event.

Let us consider $\boldsymbol{X}_i \in \mathbb{C}^{N_t \times S}$ as a narrowband DFRC signal at the $i-$th epoch, where $S \geq N_t$ is the radar pulse/communication frame's length, which can be given by

$$\boldsymbol{X}_i = \boldsymbol{W}_i \boldsymbol{S}_i, \tag{1}$$

where $\boldsymbol{W}_i = [\boldsymbol{w}_{1,i}, \cdots, \boldsymbol{w}_{M,i}]$ is the DFRC beamforming matrix required to be designed in which $\boldsymbol{w}_{j,i}$ is the $j-$th beamforming vector at the $i-$th epoch and $\boldsymbol{S}_i \in \mathbb{C}^{M \times S}$ is the data stream at the $i-$th epoch. We assume that the data streams are independent of each other, thus

$$\frac{1}{S} \boldsymbol{S}_i \boldsymbol{S}_i^H \approx \boldsymbol{I}_{N_t}, \tag{2}$$

which asymptotically holds when signaling follows a Gaussian distribution and S is sufficiently large.

A. Radar System Model

The reflected signal, $\boldsymbol{Y}_i^r \in \mathbb{C}^{N_r \times S}$, from the targets at the i-th epoch can be written as

$$\boldsymbol{Y}_i^r = \boldsymbol{G}_i \boldsymbol{X}_i + \boldsymbol{\Omega}_i, \tag{3}$$

where $\boldsymbol{G}_i \in \mathbb{C}^{N_r \times N_t}$ is the target response matrix and $\boldsymbol{\Omega}_i \in \mathbb{C}^{N_r \times S}$ is the additive white Gaussian noise (AWGN) matrix with variance σ_r^2 for each entry at the i-th epoch. Assuming a colocated MIMO radar, the target response matrix at the i-th epoch can be given by [26]

$$\boldsymbol{G}_i = \sum_{k=1}^{K} \alpha_{k,i} \boldsymbol{a}(\theta_{k,i}) \boldsymbol{b}^H(\theta_{k,i}), \tag{4}$$

where $\alpha_{k,i}$ is the complex coefficient that incorporates the two-way channel amplitude and the radar cross-section for the k-th target at the i-th epoch and $\theta_{k,i}$ represents both the angle of departure (AoD) and angle of arrival (AoA) of the k-th target at the i-th epoch because the transmitter and receiver antennas are approximately located at the same point. Moreover, $\boldsymbol{a}(\theta) = [1, e^{j\frac{2\pi}{\lambda} d \sin(\theta)}, \cdots, e^{j\frac{2\pi}{\lambda} d(N_t-1)\sin(\theta)}]^T$, and $\boldsymbol{b}(\theta) = [1, e^{j\frac{2\pi}{\lambda} d \sin(\theta)}, \cdots, e^{j\frac{2\pi}{\lambda} d(N_r-1)\sin(\theta)}]^T$, are the steering vectors associated with the transmit and receiver antennas, respectively, where λ and d are the wavelength of the signal and antenna spacing, respectively. Without loss of

generality, in this paper, we assume that $d = \frac{\lambda}{2}$. Consequently, the covariance of the radar channel at the $i-$th epoch can be written as

$$\boldsymbol{R}_i = \sum_{k=1}^{K} \sigma_{i,k}^2 \big(\boldsymbol{b}(\theta_{k,i}) \otimes \boldsymbol{a}(\theta_{k,i})\big)\big(\boldsymbol{b}(\theta_{k,i}) \otimes \boldsymbol{a}(\theta_{k,i})\big)^H, \quad (5)$$

where $\sigma_{i,k}^2 = \mathbb{E}\{\alpha_{k,i}\alpha_{k,i}^H\}$ is the expected strength of the k-th target at the i-th epoch.

For the radar performance, we use the mutual information between the received echo signal and the radar channel at the $i-$th epoch, $I(\boldsymbol{Y}_i^r; \boldsymbol{G}_i)$, which can be defined as [36]

$$\begin{aligned} I(\boldsymbol{Y}_i^r; \boldsymbol{G}_i) &= H(\boldsymbol{Y}_i^r) - H(\boldsymbol{Y}_i^r|\boldsymbol{G}_i) \\ &= \log\det(\boldsymbol{I}_{N_t} + \sigma_r^{-2}\boldsymbol{R}_i\boldsymbol{X}_i\boldsymbol{X}_i^H), \end{aligned} \quad (6)$$

where $H(\boldsymbol{Y}) = \int P(\boldsymbol{Y})\log(P(\boldsymbol{Y}))d\boldsymbol{Y}$ is the differential entropy of $\boldsymbol{Y}$ in which $P(\boldsymbol{Y})$ is the probability density function (PDF) of $\boldsymbol{Y}$. Moreover, $H(\boldsymbol{Y}|\boldsymbol{G}) = \int P(\boldsymbol{Y}|\boldsymbol{G})\log P(\boldsymbol{Y}|\boldsymbol{G})d\boldsymbol{Y}$ shows the conditional differential entropy of $\boldsymbol{Y}$ constrained on $\boldsymbol{G}$ where $P(\boldsymbol{Y}|\boldsymbol{G})$ is the conditional PDF of $\boldsymbol{Y}$ conditioned on $\boldsymbol{G}$. Note that for obtaining equation (6), $\det(\boldsymbol{I} + \boldsymbol{AB}) = \det(\boldsymbol{I} + \boldsymbol{BA})$ is used. It is worth mentioning that the justification for using the mutual information as the MIMO radar performance metric has been extensively studied in [31]–[34] and references therein.

B. Communication System Model

From the communication perspective, we consider two cases, single-target and multiple targets scenarios in the following subsections.

C. Single-Target Scenario

The received signal $\boldsymbol{Y}_i^c \in \mathbb{C}^{M\times S}$ for the single-target case at the i-th epoch can be given by

$$\boldsymbol{Y}_i^c = \boldsymbol{H}_i^H\boldsymbol{X}_i + \boldsymbol{N}_i, \quad (7)$$

where $\boldsymbol{N}_i \in \mathbb{C}^{M\times S}$ denotes the AWGN matrix at the i-th epoch with variance σ_c^2 for each entry. Moreover, $\boldsymbol{H}_i = [\boldsymbol{h}_{1,i}, \cdots, \boldsymbol{h}_{M,i}] \in \mathbb{C}^{N_t\times M}$ is the communication channel matrix where $\boldsymbol{h}_{j,i} \in \mathbb{C}^{N_t}, \forall j \in \{1, \cdots, M\}$ is the communication channel for the $j-$the user at the i-th epoch. Then, the SINR at the i-epoch for the $m-$the user can be given by

$$\gamma_{m,i} = \frac{|\boldsymbol{h}_{m,i}^H\boldsymbol{w}_{m,i}|^2}{\sum_{j\neq m}|\boldsymbol{h}_{m,i}^H\boldsymbol{w}_{j,i}|^2 + \sigma_c^2}, \quad (8)$$

where the term $\sum_{j\neq m}|\boldsymbol{h}_{m,i}^H\boldsymbol{w}_{j,i}|^2$ represents the interference term from other users at the $m-$the user.

D. Multiple Targets Scenario

For the multiple targets scenario, we add K beamforming vectors to $\boldsymbol{W}_i = [\boldsymbol{w}_{1,i}, \cdots, \boldsymbol{w}_{K+M,i}]$, where the first M vectors are communication beamformers and the last K vectors are the auxiliary beamformers to enable the extra radar probing signals the i-th epoch. Consequently, the SINR can be reformulated as

$$\gamma_{m,i} = \frac{|\boldsymbol{h}_{m,i}^H\boldsymbol{w}_{m,i}|^2}{\sum_{j\neq m}^{M+K}|\boldsymbol{h}_{m,i}^H\boldsymbol{w}_{j,i}|^2 + \sigma_c^2}. \quad (9)$$

Note that in Section III, we clarify the difference between the single-target and multiple targets scenarios in our proposed DFRC designs and why we added auxiliary beamformers for the multiple targets scenario.

E. Energy Modeling and Balancing

From the energy arrival point of view, the DFRC designs require to satisfy two conditions, the casualty and battery overflow constraints [20]–[25]. The causality constraint states that the harvested energy must not be consumed before being collected, which can be guaranteed with the following linear constraints

$$\sum_{i=1}^{k}\left(\sum_{j=1}^{M}\|\boldsymbol{w}_{j,i}\|_2^2\right)\ell_i \leq \sum_{i=1}^{k}E_{in}[i], \quad k \in \{1, \cdots, L_E\}, \quad (10)$$

where E_{in} represents the energy level at each epoch, with $E_{in}[1] = E[0]$ and $E_{in}[i] = E[j]$ if the event is the energy arrival in which $E[j]$ is the $j-$th energy arrival, otherwise, $E_{in}[i] = 0$, as shown this in Fig. 2. If the difference of energy arrival rates (EAR)s and consumed energy is less than the battery capacity, the excessive energy must be utilized for the communication or radar tasks to avoid an overflow at the battery. This can be ensured by the following linear constraints as [23]

$$\sum_{i=1}^{k}E_{in}[i] - \sum_{i=1}^{k}\left(\sum_{j=1}^{M}\|\boldsymbol{w}_{j,i}\|_2^2\right)\ell_i \leq E_{\max}, k \in \{1, \cdots, L_E\}. \quad (11)$$

F. Problem Formulation

Our aim is, using the above modeling, to design a signaling methodology for the DFRC-AP that enables net-zero energy operation. Accordingly, we formulate the below optimization problems where we aim to jointly maximize the radar mutual information and minimum QoS of the communication users subject to the energy constraints over the whole operation time. Exploiting the fact that $\boldsymbol{X}_i\boldsymbol{X}_i^H = \sum_{j=1}^{M}\boldsymbol{w}_{j,i}\boldsymbol{w}_{j,i}^H$ and discretizing the transmission time to L_E epochs, we propose the following optimization problem

$$\begin{aligned} \max_{\substack{\boldsymbol{w}_{j,i}, R \\ \forall j,i}} \quad & (1-\eta)\sum_{i=1}^{L_E}\log\det\left[\boldsymbol{I}_{N_t} + \sigma_r^{-2}\boldsymbol{R}_i\left(\sum_{j=1}^{M}\boldsymbol{w}_{j,i}\boldsymbol{w}_{j,i}^H\right)\right] \\ & + \eta R \\ \text{s.t. } & (10) \text{ and } (11), \\ & \log\left(1 + \frac{|\boldsymbol{h}_{m,i}^H\boldsymbol{w}_{m,i}|^2}{\sum_{j\neq m}^{M}|\boldsymbol{h}_{m,i}^H\boldsymbol{w}_{j,i}|^2 + \sigma_c^2}\right) \geq R, \ \forall m, i, \end{aligned} \quad (12a)$$

where the objective value jointly maximizes the radar mutual information and minimum QoS of the communication users

with the regularization parameter, $\eta > 0$. Note that η is not an optimization variable but it can be pre-determined to strike a balance between the radar and communication performances. Constraint (12a) ensures fairness among the communication users by applying a minimum rate threshold R. By maximizing R in the objective value, the proposed optimization maximizes this communication QoS threshold over the whole transmission interval. Solving (12) is non-trivial because the product structure of variables and co-channel interference among the radar targets and communication users, which makes the problem non-convex. To tackle these issues, let us first define

$$\boldsymbol{W}_{j,i} = \boldsymbol{w}_{j,i}\boldsymbol{w}_{j,i}^H, \quad \boldsymbol{Q}_{j,i} = \boldsymbol{h}_{j,i}\boldsymbol{h}_{j,i}^H, \tag{13}$$

then, we can write

$$\begin{aligned} \|\boldsymbol{w}_{j,i}\|_2^2 &= \mathrm{tr}(\boldsymbol{w}_{j,i}\boldsymbol{w}_{j,i}^H) \\ &= \mathrm{tr}(\boldsymbol{W}_{j,i}), \\ |\boldsymbol{h}_{j,i}^H\boldsymbol{w}_{j,i}|^2 &= \mathrm{tr}(\boldsymbol{h}_{j,i}^H\boldsymbol{w}_{j,i}\boldsymbol{h}_{j,i}^H\boldsymbol{w}_{j,i}) \\ &= \mathrm{tr}(\boldsymbol{h}_{j,i}\boldsymbol{h}_{j,i}^H\boldsymbol{w}_{j,i}\boldsymbol{w}_{j,i}^H) \\ &= \mathrm{tr}(\boldsymbol{Q}_{j,i}\boldsymbol{W}_{j,i}), \\ \sum_{j=1}^{M}\boldsymbol{w}_{j,i}\boldsymbol{w}_{j,i} &= \sum_{j=1}^{M}\boldsymbol{W}_{j,i}. \end{aligned} \tag{14}$$

Then, problem (12) can be recast as

$$\begin{aligned} \max_{\substack{\boldsymbol{w}_{j,i},R \\ \forall j,i}} \ & (1-\eta)\sum_{i=1}^{L_E}\log\det\left[\boldsymbol{I}_{N_t} + \sigma_r^{-2}\boldsymbol{R}_i\left(\sum_{j=1}^{M}\boldsymbol{W}_{j,i}\right)\right] \\ & + \eta R \\ \text{s.t. } & \sum_{i=1}^{k}\left(\sum_{j=1}^{M}\mathrm{tr}(\boldsymbol{W}_{j,i})\right)\ell_i \le \sum_{i=1}^{k}E_{in}[i], \\ & k \in \{1,\cdots,L_E\}, \qquad (15a) \\ & \sum_{i=1}^{k}E_{in}[i] - \sum_{i=1}^{k}\left(\sum_{j=1}^{M}\mathrm{tr}(\boldsymbol{W}_{j,i})\right)\ell_i \le E_{\max}, \\ & k \in \{1,\cdots,L_E\}, \qquad (15b) \\ & \log\left(1 + \frac{\mathrm{tr}(\boldsymbol{Q}_{m,i}\boldsymbol{W}_{m,i})}{\sum_{j\neq m}^{M}\mathrm{tr}(\boldsymbol{Q}_{m,i}\boldsymbol{W}_{j,i}) + \sigma_c^2}\right) \ge R, \ \forall m,i, \qquad (15c) \\ & \boldsymbol{W}_{j,i} \succeq 0, \ \mathrm{rank}(\boldsymbol{W}_{j,i}) = 1, \ \forall j \in \{1,\cdots,M\}, i. \qquad (15d) \end{aligned}$$

The above optimization is a non-deterministic polynomial-time (NP)-hard problem because of the fractional structure of constraints (15c) and non-convex rank constraints in (15d).

The following sections are dedicated to addressing this, where we first consider the single-target scenario and then study the multiple targets scenario when full CSI and EAI are assumed to be known at the DFRC-AP. It is worth highlighting the value of this scenario. The performance obtained for the full CSI and EAI scenario can be considered as a reference upper-bound performance because this obtains the best performance for any feasible DFRC designs. Therefore, our proposed robust DFRC designs can be compared with this scenario. Moreover, these assumptions help to find out optimal solution structures and gives insights into the optimal system design, which can be used for developing our robust DFRC designs in Section IV. This has been widely used in the EH communication literature in [20]–[25] and references therein.

III. Net-Zero Energy DFRC-AP Design Under Full CSI and EAI

In this section, we assume that full CSI and EAI are available at the AP to obtain the reference performance. As mentioned, there is no efficient solution for solving problem (15) as it contains the non-convex constraints. However, in the following, we tackle non-convex issues one by one. To relax the non-convexity of (15c), let us rewrite this constraint as

$$\begin{aligned} & \log_2\left(\sum_{j=1}^{M}\mathrm{tr}(\boldsymbol{Q}_{m,i}\boldsymbol{W}_{j,i}) + \sigma_c^2\right) \\ & - \log_2\left(\sum_{j\neq m}^{M}\mathrm{tr}(\boldsymbol{Q}_{m,i}\boldsymbol{W}_{j,i}) + \sigma_c^2\right) \ge R, \forall \ m,i, \end{aligned} \tag{16}$$

which is still non-convex as it is the summation of convex and concave functions. Here, we adapt the successive convex approximation approach to achieve a locally convex form for this constraint. It is worth noting that each convex function, $f(\boldsymbol{t})$, at the local point, $\tilde{\boldsymbol{t}}$, can be linearly lower bounded by [37]

$$f(\boldsymbol{t}) \ge f(\tilde{\boldsymbol{t}}) + \nabla_{\boldsymbol{t}} f(\tilde{\boldsymbol{t}})^T(\boldsymbol{t} - \tilde{\boldsymbol{t}}). \tag{17}$$

As a result, the second term of the left-hand side of (16) at the local points, $\tilde{\boldsymbol{W}}_{j,i}, \forall j,i$, can be bounded by

$$\begin{aligned} & -\log_2\left(\sum_{j\neq m}^{M}\mathrm{tr}(\boldsymbol{Q}_{m,i}\boldsymbol{W}_{j,i}) + \sigma_c^2\right) \\ & \ge -\log_2\left(\sum_{j\neq m}^{M}\mathrm{tr}(\boldsymbol{Q}_{m,i}\tilde{\boldsymbol{W}}_{j,i}) + \sigma_c^2\right) \\ & - \sum_{j\neq m}^{M}\mathrm{tr}\left(\frac{\boldsymbol{Q}_{m,i}(\boldsymbol{W}_{j,i} - \tilde{\boldsymbol{W}}_{j,i})}{(\sum_{r\neq m}\mathrm{tr}(\boldsymbol{Q}_{m,i}\tilde{\boldsymbol{W}}_{r,i}) + \sigma_c^2)\ln 2}\right). \end{aligned} \tag{18}$$

By dropping the rank-one constraints in (15) and using the derived bound in (18), problem (15) can be recast as

$$\begin{aligned}
\max_{\substack{\boldsymbol{w}_{j,i},R\\ \forall j,i}}\ & (1-\eta)\sum_{i=1}^{L_E}\log\det\left[\boldsymbol{I}_{N_t}+\sigma_r^{-2}\boldsymbol{R}_i\Big(\sum_{j=1}^{M}\boldsymbol{W}_{j,i}\Big)\right]\\
&+\eta R\\
&\text{s.t. }\sum_{i=1}^{k}\left(\sum_{j=1}^{M}\mathrm{tr}(\boldsymbol{W}_{j,i})\right)\ell_i\le\sum_{i=1}^{k}E_{in}[i],\\
&k\in\{1,\cdots,L_E\},\qquad (19a)\\
&\sum_{i=1}^{k}E_{in}[i]-\sum_{i=1}^{k}\left(\sum_{j=1}^{M}\mathrm{tr}(\boldsymbol{W}_{j,i})\right)\ell_i\le E_{\max},\\
&k\in\{1,\cdots,L_E\},\qquad (19b)\\
&\log_2\left(\sum_{j=1}^{M}\mathrm{tr}(\boldsymbol{Q}_{m,i}\boldsymbol{W}_{j,i})+\sigma_c^2\right)\\
&-\log_2\left(\sum_{j\neq m}^{M}\mathrm{tr}(\boldsymbol{Q}_{m,i}\tilde{\boldsymbol{W}}_{j,i})+\sigma_c^2\right)\\
&-\sum_{j\neq m}^{M}\mathrm{tr}\left(\frac{\boldsymbol{Q}_{m,i}(\boldsymbol{W}_{j,i}-\tilde{\boldsymbol{W}}_{j,i})}{(\sum_{r\neq m}\mathrm{tr}(\boldsymbol{Q}_{m,i}\tilde{\boldsymbol{W}}_{r,i})+\sigma_c^2)\ln 2}\right)\ge R,\\
&\forall m,i,\qquad (19c)\\
&\boldsymbol{W}_{j,i}\succeq 0,\ \forall j\in\{1,\cdots,M\},i.\qquad (19d)
\end{aligned}$$

which is convex, hence, it can be efficiently solved using interior-point methods exploited by the numerical convex solvers such as CVX [38]. It is worth clarifying that the feasible set of (19) is a subset of the feasible set of (12) using the derived bound in (18). Therefore, the objective value of problem (12) severs as an upper bound for the objective value of (19).

Now, we deal with the rank-one constraints dropped from the original problem. In the following theorem, we show that the rank of the optimal solutions of problem (19) is upper bounded by the number of targets.

***Theorem** 1:* Let $\hat{\boldsymbol{W}}_{j,i},\forall j,i$ be the optimal solutions of problem (19), for the single-target scenario, then

$$\mathrm{rank}(\hat{\boldsymbol{W}}_{j,i})=1,\quad \forall j\in\{1,\cdots,M\}. \tag{20}$$

Also, for the multiple targets scenario,

$$\mathrm{rank}(\hat{\boldsymbol{W}}_{j,i})\le K,\quad \forall j\in\{1,\cdots,M\}. \tag{21}$$

Proof: See Appendix A.

Let us first consider the single-target scenario in the following subsection.

A. Single-Target Scenario

Using Theorem 1, one can understand that though the rank-one constraints are dropped, rank-one solutions are always obtained for the single-target case from problem (19). However, there is no guarantee to achieve rank-one solutions for the multiple targets case. In the next subsection, we propose a novel technique that adds auxiliary variables to the optimization problem for achieving rank-one solutions for the beamforming matrices in the multiple targets case.

Algorithm 1: The block coordinate descent technique for the optimization problem in (19).

1: Let us initialize $\tilde{\boldsymbol{W}}_{j,i},\forall j,i$ by solving problem (19) with additional constraints $\|\boldsymbol{W}_{j,i}\|_\star\le 1,\forall j,i$, and set $t=1$, and $\epsilon\ll 1$ as the iteration step and tolerance of error, respectively.
2: **Repeat**
3: For given $\tilde{\boldsymbol{W}}_{j,i}^{t}$, solve (19), store the solution $\hat{\boldsymbol{W}}_{j,i}$ in $\tilde{\boldsymbol{W}}_{j,i}^{t+1},\forall j,i$, and set $t=t+1$.
5: **Until** $\frac{\|\tilde{\boldsymbol{W}}_{j,i}^{t}-\tilde{\boldsymbol{W}}_{j,i}^{t-1}\|}{\|\tilde{\boldsymbol{W}}_{j,i}^{t-1}\|}\le\epsilon,\forall j,i,$
Result: The beamforming matrices $\boldsymbol{W}_{j,i}^{\star}=\tilde{\boldsymbol{W}}_{j,i}^{t},\ \forall j,i.$

Note that the lower bound in (18) is derived at local points, $\tilde{\boldsymbol{W}}_{j,i},\forall j,i$, which means that the optimal solutions of problem (19) might not be tight. To tighten the beamforming solutions, we propose an iterative algorithm based on the block coordinate decent technique. We first solve problem (19) with extra constraints $\|\boldsymbol{W}_{j,i}\|_\star\le 1,\forall j,i$, in which $\|\cdot\|_\star$ is the nuclear norm in order to obtain an initial point for the algorithm. Note that the nuclear norm is the closest convex norm to rank constraints [39]. Indeed, we relax $\mathrm{rank}(\boldsymbol{W}_{j,i})=1$ with its closest convex relaxation, i.e., $\|\boldsymbol{W}_{j,i}\|_\star\le 1$. Then, we solve problem (19) and use its optimal solutions for the next iteration and repeat this iteratively. The algorithm can be terminated when $\frac{\|\tilde{\boldsymbol{W}}_{j,i}^{t}-\tilde{\boldsymbol{W}}_{j,i}^{t-1}\|_2}{\|\tilde{\boldsymbol{W}}_{j,i}^{t-1}\|_2}\le\epsilon,\forall j,i$, where ϵ is the tolerance error and t is the iteration step. We summarize the process in Algorithm 1. In the following theorem, we mathematically prove the convergence of Algorithm 1.

***Theorem** 2:* Algorithm 1 is convergent.

Proof: See Appendix B for the proof.

Here, we obtain the overall computational complexity of problem (19) as the major task of Algorithm 1. It is worth mentioning that the interior point method with the Newton step are typically used to implement convex problems in CVX [37], [40], which requires the computational complexity in the order of $\mathcal{O}\big((E+F)^{1.6}E^2\big)$, in which E and F are the numbers of variables and constraints in the optimization problem. Problem (19) contains MN_t^2+1 variables and $4L_E+2M$ constraints, then, the overall computational complexity of problem (19) can be approximated by $\mathcal{O}((MN_t^2)^{3.6}+(4L_E+2M)^{1.6}(MN_t)^2)$. Thus, Problem (19) can be implemented in practice with moderate numbers of antennas, epochs, and communication users. Now, we consider the multiple targets scenario in the following subsection.

B. Multiple Targets Scenario

For the multiple targets scenario, from (9) and defining $\boldsymbol{R}_{x,i}=\sum_{j=1}^{M+K}\boldsymbol{W}_{j,i}$, the radar mutual information can be reformulated as $I(\boldsymbol{Y}_i^r;\boldsymbol{G}_i)=\log\det(\boldsymbol{I}_{N_t}+\sigma_r^{-2}\boldsymbol{R}_i\boldsymbol{X}_i\boldsymbol{X}_i^H)=$

$\log\det\left[\boldsymbol{I}_{N_t}+\sigma_r^{-2}\boldsymbol{R}_i\boldsymbol{R}_{x,i}\right]$. Consequently, problem (19) for the multiple targets scenario can be recast as

$$\max_{\substack{\boldsymbol{R}_{x,i},\boldsymbol{w}_{m,i}\\ \forall m,i,R}} (1-\eta)\sum_{i=1}^{L_E}\log\det\left[\boldsymbol{I}_{N_t}+\sigma_r^{-2}\boldsymbol{R}_i\boldsymbol{R}_{x,i}\right]+\eta R$$

$$\text{s.t. } \sum_{i=1}^{k}\mathrm{tr}(\boldsymbol{R}_{x,i})\ell_i\le\sum_{i=1}^{k}E_{in}[i],\quad k\in\{1,\cdots,L_E\},\tag{22a}$$

$$\sum_{i=1}^{k}E_{in}[i]-\sum_{i=1}^{k}\mathrm{tr}(\boldsymbol{R}_{x,i})\ell_i\ge E_{\max},\quad k\in\{1,\cdots,L_E\},\tag{22b}$$

$$\log_2\left(\sum_{j=1}^{M+K}\mathrm{tr}(\boldsymbol{Q}_{m,i}\boldsymbol{W}_{j,i})+\sigma_c^2\right)-\log_2\left(\sum_{j\neq m}^{M+K}\mathrm{tr}(\boldsymbol{Q}_{m,i}\tilde{\boldsymbol{W}}_{j,i})+\sigma_c^2\right)-\sum_{j\neq m}^{M+K}\mathrm{tr}\left(\frac{\boldsymbol{Q}_{m,i}(\boldsymbol{W}_{j,i}-\tilde{\boldsymbol{W}}_{j,i})}{(\sum_{r\neq m}\mathrm{tr}(\boldsymbol{Q}_{m,i}\tilde{\boldsymbol{W}}_{r,i})+\sigma_c^2)\ln 2}\right)\ge R,\quad\forall m,i,\tag{22c}$$

$$\boldsymbol{R}_{x,i}\succeq\sum_{m=1}^{M}\boldsymbol{W}_{m,i},\boldsymbol{W}_{j,i}\succeq 0,\quad\forall j\in\{1,\cdots,M+K\},i,\tag{22d}$$

where is convex and can be efficiently solved using CVX. The solutions of the above problem are tight if $\mathrm{rank}(\boldsymbol{W}_{j,i})=1,\forall j\in\{1,\cdots,M\},i$. However, the beamforming matrices are not necessarily rank-one. Thus, we provide the following theorem to show that one can always find tight solutions from the optimal solutions of problem (22).

***Theorem** 3:* There exists global optimal solutions for problem (22) as

$$\bar{\boldsymbol{w}}_{j,i}=(\boldsymbol{h}_{j,i}^H\hat{\boldsymbol{W}}_{j,i}\boldsymbol{h}_{j,i})^{-1/2}\hat{\boldsymbol{W}}_{j,i}\boldsymbol{h}_{j,i},\bar{\boldsymbol{W}}_{j,i}=\bar{\boldsymbol{w}}_{j,i}\bar{\boldsymbol{w}}_{j,i}^H,\quad\forall j\in\{1,\cdots,M\},\ \bar{\boldsymbol{R}}_{x,i}=\hat{\boldsymbol{R}}_{x,i},\quad\forall i,\tag{23}$$

where $\hat{\boldsymbol{W}}_{j,i},\forall j\in\{1,\cdots,M\}$ and $\hat{\boldsymbol{R}}_{x,i}$ are the optimal solutions of problem (22).

Proof: See Appendix 3.

Building on the approach explained in Subsection III-A for the single-target scenario, we tighten the solutions of optimization problem (22). To avoid excessive clutter, we do not write the algorithm for the multiple targets scenario and use the process of Algorithm 1 with a little change. More precisely, for the first step of Algorithm 1, constraints $\|\boldsymbol{W}_{j,i}\|_\star\le 1,\forall j\in\{1,\cdots,M\},i$, must be changed to $\|\boldsymbol{W}_{j,i}\|_\star\le K,\forall j\in\{1,\cdots,M\},i$, to align with the K targets. The convergence also can be straightforwardly proved using Theorem 2.

Now, we derive the total computational complexity of problem (22 for the multiple targets scenario. Building on the complexity of solving convex problem, the total computational complexity of problem (22) can be approximated by $\mathcal{O}(((M+K)N_t^2)^{3.6}+(4L_E+2M+K)^{1.6}(MN_t)^2)$, which shows that problem (22) is implementable in practice. In the next section, we consider the case when only imperfect CSI and EAI are available at the AP.

IV. Robust Net-Zero Energy DFRC-AP Design

In the previous sections, by assuming full CSI and EAI at the AP, we have obtained reference designs for both the single-target and multiple targets scenarios. However, in practice, only imperfect information about the CSI and EAI are available because the AP is not aware of the future events (changes in the channel states and energy arrivals). Thus, in this section, we propose a RD optimization for the case where only imperfect CSI and EAI are assumed to be known at the DFRC-AP.

Let us first determine the average number of events and their length during the transmission interval using the prior statistical knowledge about the events. Exploiting the fact that the combination of three independent Poisson processes with rates λ_1, λ_2, and λ_3 is still a Poisson process with rate $\lambda_1+\lambda_2+\lambda_3$, the number of events during the transmission interval can be modeled as a a Poisson process with rate $\lambda_e+\lambda_c+\lambda_r$. Consequently, the average number of events and their length can be obtained as $\bar{L}_E=T(\lambda_e+\lambda_c+\lambda_r)$, $\bar{\ell}=\frac{T}{\bar{L}_E}$, respectively.

Regarding the optimization problem in (12), the optimal DFRC design depends on the covariance of the two-way radar channel, communication channel, and energy arrivals information. Thus, we assume that radar and communication channels are available at the AP with certain errors as

$$\dot{\boldsymbol{G}}_i=\boldsymbol{G}_i+\boldsymbol{V}_i,\quad\dot{\boldsymbol{h}}_{m,i}=\boldsymbol{h}_{m,i}+\boldsymbol{q}_{m,i},\quad\forall i,m.\tag{24}$$

in which $\|\boldsymbol{q}_{m,i}\|_2\le\delta_c,\forall m,i$ and $\|\boldsymbol{V}_i\|_2\le\delta_r$ where δ_c and δ_r are known. Note that for notation simplicity, we assume that all the users have the same errors over all the epochs. This has been assumed for the radar channels. The bound on communication channel states can be calculated through a long-term measurement in practice and the radar channel bound can be translated to prior information regarding the velocity of the targets under study.

Let us consider the worst-case scenario where the minimum mutual information and QoS provided by the minimum energy arrival values. To do so, let us first write a lower bound on the radar mutual information using the technique proposed in [41] and prior information regarding the radar channel in (24)

as

$$\begin{aligned}
&\log\det\left[\boldsymbol{I}_{N_t}+\sigma_r^{-2}\dot{\boldsymbol{G}}_i\sum_{j=1}^{M}\boldsymbol{W}_{j,i}\right]\\
&=\log\det\left[\boldsymbol{I}_{N_t}+\sigma_r^{-2}\Big(\boldsymbol{G}_i\boldsymbol{G}_i^H-\boldsymbol{G}_i^H\boldsymbol{V}_i-\boldsymbol{V}_i^H\boldsymbol{G}_i\right.\\
&\left.+\boldsymbol{V}_i^H\boldsymbol{V}_i\Big)\sum_{j=1}^{M}\boldsymbol{W}_{j,i}\right]\\
&\geq\log\det\left[\boldsymbol{I}_{N_t}+\sigma_r^{-2}\Big(\boldsymbol{G}_i\boldsymbol{G}_i^H\right.\\
&\left.(-2\delta_r\|\boldsymbol{G}_i\|_2+\delta_r^2)\boldsymbol{I}\Big)\sum_{j=1}^{M}\boldsymbol{W}_{j,i}\right].
\end{aligned}\tag{25}$$

Similarly, the lower bound on the communication rate can be given by

$$\begin{aligned}
&\min_{\|\boldsymbol{q}_{m,i}\|_2\leq\delta_c}\log\left(1+\frac{|\dot{\boldsymbol{h}}_{m,i}^H\boldsymbol{w}_{m,i}|^2}{\sum_{j\neq m}^{M}|\dot{\boldsymbol{h}}_{m,i}^H\boldsymbol{w}_{j,i}|^2+\sigma_c^2}\right)\\
&=\min_{\|\boldsymbol{q}_{m,i}\|_2\leq\delta_c}\log\left(1+\frac{|(\boldsymbol{h}_{m,i}^H+\boldsymbol{q}_{m,i}^H)\boldsymbol{w}_{m,i}|^2}{\sum_{j\neq m}^{M}|(\boldsymbol{h}_{m,i}^H+\boldsymbol{q}_{m,i}^H)\boldsymbol{w}_{j,i}|^2+\sigma_c^2}\right)\\
&\leq\log\left(1+\frac{\min_{\|\boldsymbol{q}_{m,i}\|_2\leq\delta_c}|(\boldsymbol{h}_{m,i}^H+\boldsymbol{q}_{m,i}^H)\boldsymbol{w}_{m,i}|^2}{\sum_{j\neq m}^{M}\max_{\|\boldsymbol{q}_{m,i}\|_2\leq\delta_c}|(\boldsymbol{h}_{m,i}^H+\boldsymbol{q}_{m,i}^H)\boldsymbol{w}_{j,i}|^2+\sigma_c^2}\right)\\
&\leq\log\left(1+\frac{\mathrm{tr}(\dot{\boldsymbol{Q}}_{m,i}\boldsymbol{W}_{m,i})}{\sum_{j\neq m}^{M}\mathrm{tr}(\breve{\boldsymbol{Q}}_{m,i}\boldsymbol{W}_{j,i})+\sigma_c^2}\right),
\end{aligned}\tag{26}$$

where $\dot{\boldsymbol{Q}}_{m,i}=\boldsymbol{h}_{m,i}\boldsymbol{h}_{m,i}^H+(\delta_c^2-2\delta_c\|\boldsymbol{h}_{m,i}\|_2)\boldsymbol{I}$ and $\breve{\boldsymbol{Q}}_{m,i}=\boldsymbol{h}_{m,i}\boldsymbol{h}_{m,i}^H+(\delta_c^2+2\delta_c\|\boldsymbol{h}_{m,i}\|_2)\boldsymbol{I}$.

Here, we deal with the energy arrival values. As mentioned, in this paper, we assume that the energy arrival values follow a uniform distribution, i.e., $E[i]\backsim U(e_{\min},e_{\max})$ for $i\in\{1,\cdots,L_e\}$. Note that the bound on energy arrival values can be determined using some prior information about the environment where the DFRC-AP is employed. For example, for the solar panels, since the panel sizes are known and precise knowledge about the environment temperature is available from meteorological stations, the output of the solar panels can be estimated with a good confidence interval at the DFRC-AP. Thus, to ensure that the RDs work for all the energy arrival values, we assume the worst-case scenario in which $E[i]=e_{\min},\forall i$. Then, by defining $\breve{\boldsymbol{G}}_i=\boldsymbol{G}_i\boldsymbol{G}_i^H(-2\delta_r\|\boldsymbol{G}_i\|_2+\delta_r^2)\boldsymbol{I}$, the original problem in (15) for the robust optimization can be recast as

$$\begin{aligned}
\max_{\substack{\boldsymbol{w}_{j,i},R\\ \forall j,i}}\ &(1-\eta)\sum_{i=1}^{\bar{L}_E}\log\det\left[\boldsymbol{I}_{N_t}+\sigma_r^{-2}\breve{\boldsymbol{G}}_i\Big(\sum_{j=1}^{M}\boldsymbol{W}_{j,i}\Big)\right]\\
&+\eta R\\
&\text{s.t.}\ \sum_{i=1}^{k}\left(\sum_{j=1}^{M}\mathrm{tr}(\boldsymbol{W}_{j,i})\right)\bar{\ell}\leq\sum_{i=1}^{k}E_{in}[i],\\
&k\in\{1,\cdots,\bar{L}_E\},\qquad(27a)\\
&\sum_{i=1}^{k}E_{in}[i]-\sum_{i=1}^{k}\left(\sum_{j=1}^{M}\mathrm{tr}(\boldsymbol{W}_{j,i})\right)\bar{\ell}\leq E_{\max},\\
&k\in\{1,\cdots,\bar{L}_E\},\qquad(27b)\\
&\log\left(1+\frac{\mathrm{tr}(\dot{\boldsymbol{Q}}_{m,i}\boldsymbol{W}_{m,i})}{\sum_{j\neq m}^{M}\mathrm{tr}(\breve{\boldsymbol{Q}}_{m,i}\boldsymbol{W}_{j,i})+\sigma_c^2}\right)\geq R,\ \forall m,i,\\
&\qquad(27c)\\
&\boldsymbol{W}_{j,i}\succeq 0,\ \mathrm{rank}(\boldsymbol{W}_{j,i})=1,\forall j,i.\qquad(27d)
\end{aligned}$$

where $E_{in}[1]=E[0]$ and $E_{in}[i]=e_{\min}$ if the event is the energy arrival, otherwise, $E_{in}[i]=0$. The problem is convex and can be solved using CVX. Regarding the definition of $\breve{\boldsymbol{G}}_i$ and the fact that $\mathrm{rank}(\boldsymbol{AB})\leq\min\{\mathrm{rank}(\boldsymbol{A}),\mathrm{rank}(\boldsymbol{B})\}$, $\breve{\boldsymbol{G}}_i$ is an $K-$rank matrix. Thus, the result of Theorem 1 is valid for the robust scenario. Consequently, the process explained in Section III can be repeated to obtain the single- and multiple-target beamforming matrices for the robust scenario.

Using the complexity of solving convex problems, the overall computational complexity of problem (27) for the single-target scenario can be approximately given by $\mathcal{O}((MN_t^2)^{3.6}+(4\bar{L}_E+2M)^{1.6}(MN_t)^2)$ by dropping the rank-one constraints. Moreover, for the multiple targets scenario, the overall computational complexity can be written as $\mathcal{O}(((M+K)N_t^2)^{3.6}+(4\bar{L}_E+2M+K)^{1.6}(MN_t)^2)$. These derivations show that the proposed RDs can be employed in practice.

V. Simulation Results

In this section, Monte Carlo simulations are done to investigate the performance of the proposed DFRC designs. We consider a MIMO AP with $N_t=N_r=10$. We assume that the power of AWGN for both communication and radar channels is normalized to 1. The spectral bandwidth is assumed to be 1 mega Hertz (MHz), then the communication rate is in megabits per second per Hertz (Mbits/s/Hz). For the communication channel, a Rayleigh channel model with complex normal variables (mean and variance $\mu_h=10^{-5}$ and $\sigma_h=10^{-10}$, respectively) is used. The results of this paper can be extended to the geometric channel model for the upcoming millimeter wave signaling. The radar channel is randomly generated, following the process proposed in [42]. We set $\epsilon=10^{-4}$ in Algorithm 1. For ease of illustration, in this section, we define the normalized radar mutual information as $\frac{1}{(L_E+1)K}\log\det(\boldsymbol{I}_{N_t}+\sigma_r^{-2}\boldsymbol{R}_i\boldsymbol{X}_i\boldsymbol{X}_i^H)$.

A. Beampatterns

We commence our evaluations by plotting the DFRC beampatterns, $\boldsymbol{a}^H(\cdot)\left[\sum_{j=1}^{M+K}\boldsymbol{W}_j\right]\boldsymbol{a}(\cdot)$, in dBi for different values

This article has been accepted for publication in IEEE Transactions on Green Communications and Networking. This is the author's version which has not been fully edited and content may change prior to final publication. Citation information: DOI 10.1109/TGCN.2023.3236029

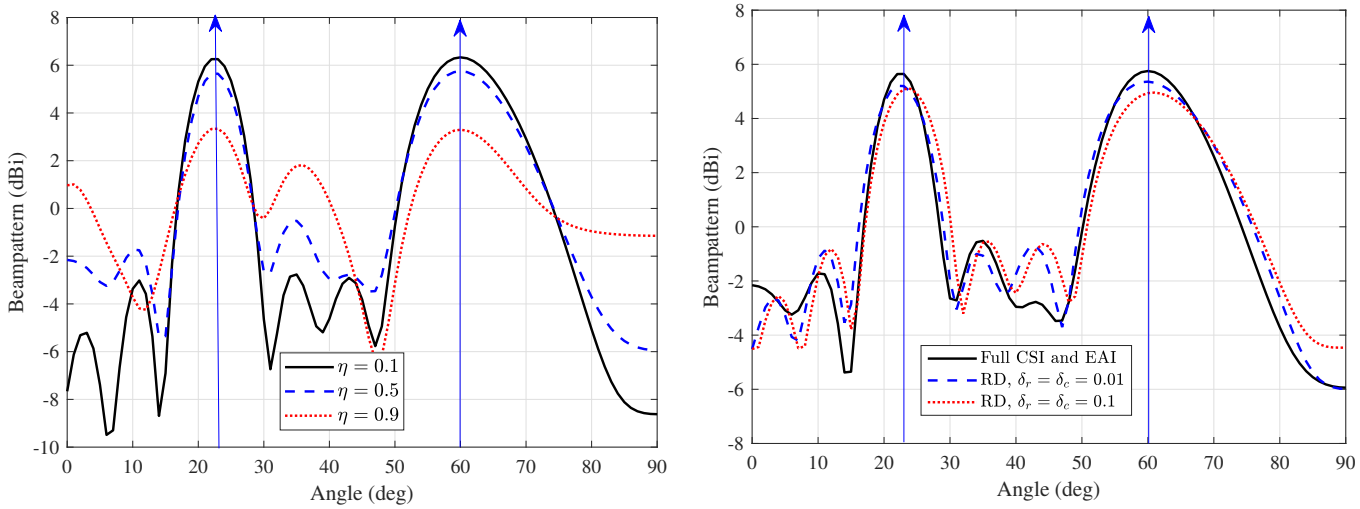

Fig. 3: Beampatterns for $K = M = 2$ and $E_{\max} = 20$ J. Fig. 3(a) shows the beampatterns for the full CSI and EAI scenario for different values of η. Fig. 3(b) compares the beampatterns of the RDs with the full CSI and EAI scenario for $\eta = 0.5$. The targets are shown by the blue arrows in both figures.

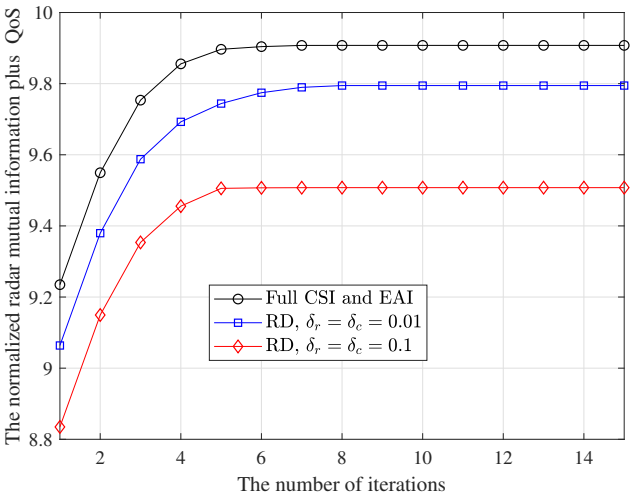

Fig. 4: The normalized radar mutual information plus minimum communication QoS normalized by the bandwidth of the system for $T = 5$ s and $\eta = 0.5$ to evaluate the convergence behavior of the proposed DFRC designs.

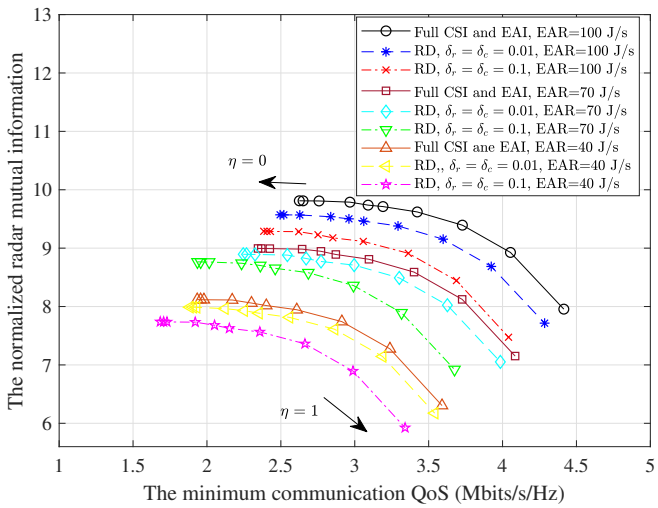

Fig. 5: The normalized radar mutual information versus the minimum communication QoS for the different values of η, $T = 5$ s, $M = K = 2$, $\lambda_c = \lambda_r = \lambda_e = 1$, $E_{\max} = 20$ for full CSI ane EAI and robust scenarios.

of η. To avoid excessive clutter, we only focus on the case where no events happen. Indeed, the required energy for the DFRC-AP comes from the stored energy at the battery, which is 100 joule (J), i.e., $E_{in}[1] = 100$ J. We assume that $T = 1$ second (s), $K = M = 2$, and $E_{\max} = 20$ J. The targets are located at $\theta_1 = \frac{\pi}{3}$ and $\theta_2 = \frac{\pi}{8}$.

Fig. 3(a) demonstrates that all three beamformers correctly focus on the main lobes where the targets exist and have random fluctuations in side lobe regions for providing the communication QoS. Moreover, when $\eta \to 0$ and $\eta \to 1$, the transmit power toward the radar targets increases and decreases, respectively. This is consistent with the fact that growing η increases the priority of the communication performance.

In Fig. 3(b), we compare the beampatterns of RDs with the full CSI and EAI scenario with $\eta = 0.5$. From this figure, it is observed that increasing the channel noises reduces the allocated power to the main lobes where the targets exist. Moreover, when $\delta_r = \delta_c = 0.1$, the beampattern does not correctly focus on the locations of targets because the channel errors are large. All three beampatterns show random fluctuations in side lobes because of the communication QoSs.

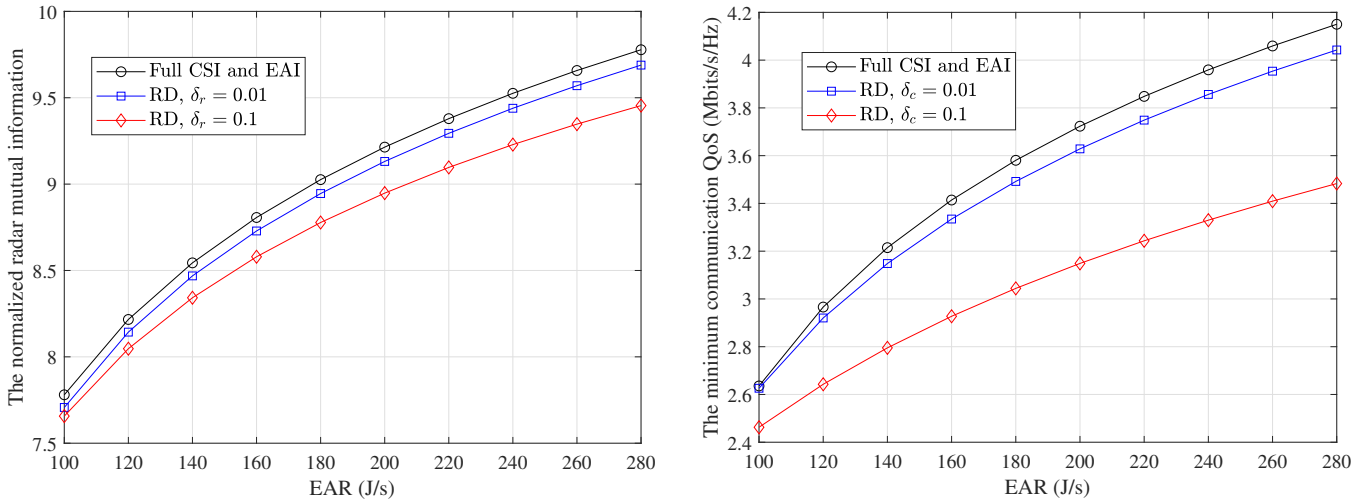

(a) (b)

Fig. 6: A comparison between the robust and full CSI and EAI scenarios in terms of the normalized radar mutual information and minimum communication QoS in Figs. 6(a) and 6(b), respectively

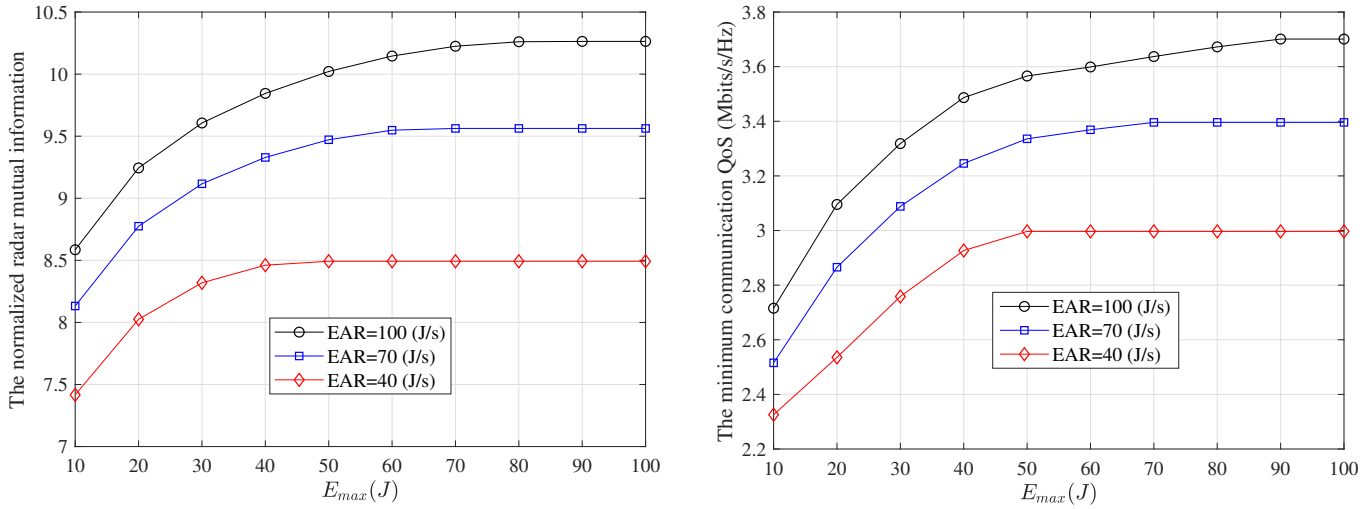

(a) (b)

Fig. 7: The radar mutual information and minimum communication QoS versus the battery size for the different values EARs in Figs. 7(a) and 7(b), respectively.

B. Convergence Behavior

In this subsection, we show that the proposed algorithm for our DFRC designs is convergent for both the full information and robust scenarios. For this simulation, we assume $T = 5$ s and $\lambda_c = \lambda_r = \lambda_e = 1$. Also, $E[i] \backsim U(35, 45)J$, $E_{\max} = 20$ J, and $M = K = 2$. Moreover, we use $\eta = 0.5$ to have a fair balance between the communication and radar performance metrics. For the robust DFRC design, we assume that the power of communication and radar channel errors are equal to 0.01 and 0.1, i.e., $\delta_c = \delta_r = 0.01$ and $\delta_c = \delta_r = 0.1$.

We plot the normalized mutual information plus the minimum communication QoS. Note that the minimum communication QoS is normalized by the bandwidth of the system for this simulation. Fig. 4 shows that both DFRC designs converge quickly with almost 7 iterations. Moreover, the performance obtained by the robust scenarios is upper bounded by the full CSI and EAI scenario and the performance reduces when the channel errors increase. Results of this figure and Theorem 2 show that the proposed DFRC designs are convergent.

C. The Radar Mutual Information Versus the Minimum Communication QoS for Different Values of η

As mentioned, the regularization parameter η offers a graceful trade-off between the communication and radar performance metrics. Thus, in this subsection, we evaluate the radar mutual information versus the communication QoS for

different values of η in order to investigate the inherent trade-off of DFRC systems under both full information and robust scenarios. We set parameters as $T = 5$s , $M = K = 2$, $\lambda_c = \lambda_r = \lambda_e = 1$, and $E_{\max} = 20$ J. Note that the EAR follows a uniform process for each point of simulations, for example, for the energy arrival 100 J/s, we have $E[i] \backsim U(95, 105)J$.

Intuitively, increasing the EARs when other variables are fixed results in better performance in terms of radar and communication metrics as there is more energy to allocate. From Fig. 5, it can be observed that the performance of all the DFRC designs increases by growing the EARs. Moreover, by growing η, the minimum communication QoS increases and the normalized radar mutual information decreases for all the DFRC designs, and vice versa. This is consistent with the results of Fig. 3. Similar to Fig. 4, the performance of the full CSI and EAI scenario serves as an upper bound for the RDs. Also, both the normalized radar mutual information and the minimum QoS decreases when the channel errors grow.

D. Robust Scenario

In this subsection, we compare the performance of our proposed robust DFRC designs with the case where full CSI and EAI are available. Note that the full CSI and EAI scenario serves as a performance benchmark as explained in Section III. For this simulation, we assume that $T = 5$ s, $M = K = 2$, $E_{\max} = 20$, and $\lambda_c = \lambda_r = \lambda_e = 1$. The robust optimization in (27) is applied to the setup of Fig. 6 yielding the average radar mutual information and minimum QoS of communication users versus the EARs. Similar to the previous simulation, the EAR follows a uniform process for each point of simulations. In order to consider imperfect communication and radar channels, two cases are studied where the errors are uniformly and randomly generated in a sphere centered at zero with radii $\delta_c = \delta_r = 0.1$ and $\delta_c = \delta_r = 0.01$ for the radar error matrices and communication error vectors.

It is observed from this figure that when the power of errors is small, $\delta_c = \delta_r = 0.01$, the performance of the robust DFRC design is comparable with the full CSI and EAI scenario. In addition, the normalized radar mutual information and the minimum QoS of communication users decrease when the power of errors increases. The reduction of the minimum QoS is more than the radar mutual information which is because of the fact that the imperfect CSI for each user directly affects their beamforming matrices, however, for the radar targets, imperfect CSI affects the covariance of the beamforming matrices as can be seen in (26) and (25), respectively. This figure highlights the practical and potential benefits of our proposed robust DFRC designs because perfect CSI and EAI scenario obtains the best performance of any feasible DFRC design.

E. Battery Size Effects

In this subsection, we show how the size of the EH battery affects the performance of the proposed DFRC designs. For this optimization, we assume that $T = 5$ s and $\lambda_c = \lambda_r = \lambda_e = 1$. We change the size of the battery for different values of EARs and plot the normalized radar mutual information and minimum communication QoS for the full CSI and EAI scenario.

Intuitively, when a larger battery is deployed, there is more space to store the harvested energies, hence, the performance is increased. The EAR is also important because when the size of the battery is larger than the EAR, the battery overflow constraints in (11) are inactive, hence, the size of the battery has no effect on the performance. This can be observed from the empirical simulations in Fig. 7. More precisely, when the size of the battery is smaller than the EARs, both the normalized radar mutual information and minimum communication QoS increase by growing the size of the battery, however, for the case where the size of the battery is larger than the EAR, both radar and communication metrics are constant and the size of the battery has not effect on the performance. In addition, by increasing the EARs for the fixed battery size, one can obtain better performance in terms of communication and radar metrics as there is more energy to consume.

VI. Conclusion and Future Research Direction

In this paper, we study the design of net-zero energy DFRC systems. We propose a non-convex problem for jointly maximizing the radar mutual information and minimum communication QoS subject to the net-zero energy constraints. We first assume that full CSI and EAI are available at the DFRC-AC to obtain the best performance achieved by any feasible beamforming matrices. We obtain the beamforming matrices for both single-target and multiple targets scenarios using the SDR and first-order Taylor expansion techniques. Then, we propose a robust optimization that only requires imperfect CSI and EAI. This can be used in the practical applications. The simulation results evaluate the performance of the proposed DFRC designs. Generalizing our proposed approaches to the massive MIMO scenario [7], [43]–[45] by reducing their implementation complexity using the alternating direction method of multipliers (ADMM), which has been studied for the communication only problems [46] is an interesting research direction to communicate and sense large numbers of users and targets using DFRC systems.

VII. Acknowledgment

This work has received funding from the European Union's Horizon 2020 research and innovation program under the Marie Skłodowska-Curie grant agreement No 812991.

APPENDIX A
PROOF OF THEOREM 1

Let us first write the Lagrangian function of problem (19) as below

$$\begin{aligned}L(\boldsymbol{l}) &= (1-\eta)\sum_{i=1}^{L_E}\log\det\left[\boldsymbol{I}_{N_t}+\sigma_r^{-2}\boldsymbol{R}_i\Big(\sum_{j=1}^{M}\boldsymbol{W}_{j,i}\Big)\right]\\ &+\eta R+\sum_{k=1}^{L_E}\mu_k\left(\sum_{i=1}^{k}\left(\sum_{j=1}^{M}\mathrm{tr}(\boldsymbol{W}_{j,i})\right)\ell_i-\sum_{i=1}^{k}E_{in}[i]\right)\\ &+\sum_{k=1}^{L_E}\phi_k\left(E_{\max}-\sum_{i=1}^{k}E_{in}[i]+\sum_{i=1}^{k}\left(\sum_{j=1}^{M}\mathrm{tr}(\boldsymbol{W}_{j,i})\right)\ell_i\right)\\ &+\sum_{k=1}^{L_E}\sum_{p=1}^{M}\psi_{k,p}\left(R-\log_2\left(\sum_{j=1}^{M}\mathrm{tr}(\boldsymbol{Q}_{m,i}\boldsymbol{W}_{j,i})+\sigma_c^2\right)\right.\\ &+\log_2\left(\sum_{j\neq m}^{M}\mathrm{tr}(\boldsymbol{Q}_{m,i}\tilde{\boldsymbol{W}}_{j,i})+\sigma_c^2\right)\\ &\left.+\sum_{j\neq m}^{M}\mathrm{tr}\left(\frac{\boldsymbol{Q}_{m,i}(\boldsymbol{W}_{j,i}-\tilde{\boldsymbol{W}}_{j,i})}{(\sum_{r\neq m}\mathrm{tr}(\boldsymbol{Q}_{m,i}\tilde{\boldsymbol{W}}_{r,i})+\sigma_c^2)\ln 2}\right)\right)\\ &+\sum_{k=1}^{L_E}\sum_{j=1}^{M}\mathrm{tr}(\boldsymbol{\Gamma}_{k,j}\boldsymbol{W}_{k,j}),\end{aligned}\tag{28}$$

where $\boldsymbol{l}$ includes all the Lagrangian variables ($\mu_k, \theta_k, \psi_{k,p}$, and $\Gamma_{k,j}, \forall k,p,j$). Then, using the sufficient and necessary Karush-Kuhn-Tucker (KKT) optimal conditions, we can take a derivative with respect to $\boldsymbol{W}_{m,i}$ as below

$$\begin{aligned}\frac{\partial L}{\partial \boldsymbol{W}_{m,i}} &= \sigma_r^{-2}(\boldsymbol{R}_i)^T\left(\boldsymbol{I}_{N_t}+\sigma_r^{-2}\boldsymbol{R}_i\Big(\sum_{j=1}^{M}\boldsymbol{W}_{j,i}\Big)\right)^{-T}\\ &+\mu_i\ell_i\boldsymbol{I}_{N_t}+\phi_i\ell_i\boldsymbol{I}_{N_t}\\ &-\psi_{m,i}\frac{\boldsymbol{Q}_{m,i}}{\sum_{j=1}^{M}\mathrm{tr}(\boldsymbol{Q}_{m,i}\boldsymbol{W}_{j,i}+\sigma_c^2)\ln 2}+\boldsymbol{\Gamma}_{m,i}.\end{aligned}\tag{29}$$

Then, for obtaining optimal solutions, the above derivative must be equal to zero, which results in

$$\begin{aligned}&(\boldsymbol{R}_i\hat{\boldsymbol{W}}_{m,i})^T\\ &=\left(\psi_{m,i}\frac{\boldsymbol{Q}_{m,i}}{\mathrm{tr}(\sum_{j\neq m}^{M}\boldsymbol{Q}_{m,i}\boldsymbol{W}_{j,i}+\boldsymbol{Q}_{m,i}\hat{\boldsymbol{W}}_{m,i}+\sigma_c^2)\ln 2}\right.\\ &\left.-\mu_i\ell_i\boldsymbol{I}_{N_t}-\phi_i\ell_i\boldsymbol{I}_{N_t}-\boldsymbol{\Gamma}_{m,i}\right)^{-1}(\boldsymbol{R}_i)^T\\ &-\sigma_r^{-2}\boldsymbol{I}_{N_t}-(\boldsymbol{R}_i\sum_{j\neq m}\boldsymbol{W}_{j,i})^T.\end{aligned}\tag{30}$$

Regarding the fact that the problem is convex, the optimal solutions are obtained at the boundary of the constraints which means that

$$\mathrm{tr}(\hat{\boldsymbol{W}}_{m,i})=\sum_{i=1}^{k}\frac{1}{\ell_i}E_{in}[i]-\sum_{i=1}^{k}\sum_{j\neq m}\mathrm{tr}(\boldsymbol{W}_{m,i}),\tag{31}$$

or

$$\mathrm{tr}(\hat{\boldsymbol{W}}_{m,i})=\sum_{i=1}^{k}\frac{1}{\ell_i}E_{in}[i]-\sum_{i=1}^{k}\sum_{j\neq m}\mathrm{tr}(\boldsymbol{W}_{m,i})-\frac{1}{\ell_i}E_{\max}.\tag{32}$$

Let us define the spectral decomposition of $\boldsymbol{R}_i$ as below

$$\boldsymbol{R}_i=\lambda_i^r\boldsymbol{r}_i\boldsymbol{r}_i^H,\tag{33}$$

where λ_i^r and $\boldsymbol{r}_i$ are the largest radar eigenvalue, and its associated unitary vectors at the $i-$th epoch. From the rank properties, we can write

$$\mathrm{rank}(\boldsymbol{R}_i\hat{\boldsymbol{W}}_{m,i})\leq\mathrm{rank}(\boldsymbol{R}_i)=1,\tag{34}$$

which means that equation (30) has N_t-1 degrees of freedom. On the other hand, $\mathrm{tr}(\boldsymbol{W}_{m,i})=\sum_{j=1}^{N_t}\lambda_{j,i}^{m,w}$ where $\lambda_{j,i}^{m}$ are the eigenvalue of the beamformer matrix for the $m-$th user at the $i-$th epoch. Then, because the optimal solutions are required to satisfy equation (30), without violating the optimization constraints, the optimal beamforming matrices can always focus on one direction where the target exists and allocate no energy to other directions. Indeed, $\lambda_{j,i}^{m,w}=0, \forall j>1, \forall i,m$, where $j=1$ is associated with the largest eigenvalue of the radar targets. This process can be repeated for all the users and epochs.

In the case of multiple targets scenario, the spectral decomposition of $\boldsymbol{R}_i$ can be given by

$$\boldsymbol{R}_i=\sum_{j=1}^{K}\lambda_{j,i}^r\boldsymbol{r}_{j,i}\boldsymbol{r}_{j,i}^H,\tag{35}$$

where $\lambda_{j,i}^r$, $\boldsymbol{r}_{j,i}$ are the radar eigenvalues and their associated unitary vectors at the $i-$th epoch, respectively. Consequently,

$$\mathrm{rank}(\boldsymbol{R}_i\hat{\boldsymbol{W}}_{m,i})\leq\mathrm{rank}(\boldsymbol{R}_i)=K,\tag{36}$$

as $K+M\leq N_t$, which suggests that the optimal beamforming matrices can focus on K directions and allocate no energy to other direction directions, N_t-K. Thus, the solutions of problem (19) for the case of multiple targets might have K-rank solutions. This concludes the proof.

APPENDIX B
PROOF OF THEOREM 2

Let us first define t and O^t as the iteration step and objective value of problem (19) at the t-th iteration, respectively. Since problem (19) solves optimally in the third step of Algorithm 1, $O^{t_3}\leq O^{t_3+1}$. Indeed, the objective value of problem (19) is increasing and upper bounded by a finite value because of the limited available energy. Therefore, Algorithm 1 converges.

APPENDIX C
PROOF OF THEOREM 3

Let us first assume that $\hat{\boldsymbol{R}}_{x,i}$ and $\hat{\boldsymbol{W}}_{j,i}, \forall j\in\{1,\cdots,M\}, i$ as the arbitrary optimal solutions of problem (22). Considering

$$\begin{aligned}\bar{\boldsymbol{w}}_{j,i}&=(\boldsymbol{h}_{j,i}^H\hat{\boldsymbol{W}}_{j,i}\boldsymbol{h}_{j,i})^{-1/2}\hat{\boldsymbol{W}}_{j,i}\boldsymbol{h}_{j,i},\\ \bar{\boldsymbol{W}}_{j,i}&=\bar{\boldsymbol{w}}_{j,i}\bar{\boldsymbol{w}}_{j,i}^H,\end{aligned}\tag{37}$$

as another optimal solutions of problem (22) guarantees that $\text{rank}(\bar{\boldsymbol{W}}_{j,i}) = 1, \forall j \in \{1, \cdots, M\}, i$. Assuming $\bar{\boldsymbol{R}}_{x,i} = \hat{\boldsymbol{R}}_{x,i}$ ensures that the first term of the objective function of problem (22) does not change also constraints (22a) and (22b) are satisfied.

To guarantee that constraints (22c), we write

$$\begin{aligned}\text{tr}(\boldsymbol{Q}_{j,i}\bar{\boldsymbol{W}}_{j,i}) &= \boldsymbol{h}_{j,i}^H \bar{\boldsymbol{W}}_{j,i}\boldsymbol{h}_{j,i} \\ &= \boldsymbol{h}_{j,i}^H \bar{\boldsymbol{w}}_{j,i}\bar{\boldsymbol{w}}_{j,i}^H \boldsymbol{h}_{j,i} \\ &= \boldsymbol{h}_{j,i}^H \hat{\boldsymbol{W}}_{j,i}\boldsymbol{h}_{j,i},\ \forall j \in \{1, \cdots, M\}, \end{aligned} \tag{38}$$

then, the first and third terms of constraint (22) can be written as

$$\begin{aligned}&\log_2\left(\sum_{j=1}^{M+K} \text{tr}(\boldsymbol{Q}_{m,i}\bar{\boldsymbol{W}}_{j,i}) + \sigma_c^2\right) \\ &= \log_2\left(\sum_{j=1}^{M} \text{tr}(\boldsymbol{Q}_{m,i}\hat{\boldsymbol{W}}_{j,i}) + \sigma_c^2\right), \\ &\sum_{j\neq m}^{M+K} \text{tr}\left(\frac{\boldsymbol{Q}_{m,i}(\bar{\boldsymbol{W}}_{j,i} - \tilde{\boldsymbol{W}}_{j,i})}{(\sum_{r\neq m} \text{tr}(\boldsymbol{Q}_{m,i}\tilde{\boldsymbol{W}}_{r,i}) + \sigma_c^2)\ln 2}\right) \\ &= \sum_{j\neq m}^{M+K} \text{tr}\left(\frac{\boldsymbol{Q}_{m,i}(\hat{\boldsymbol{W}}_{j,i} - \tilde{\boldsymbol{W}}_{j,i})}{(\sum_{r\neq m} \text{tr}(\boldsymbol{Q}_{m,i}\tilde{\boldsymbol{W}}_{r,i}) + \sigma_c^2)\ln 2}\right). \end{aligned} \tag{39}$$

This shows that $\bar{\boldsymbol{W}}_{j,i}$ lies on the feasible set of problem (22).

To ensure that $\bar{\boldsymbol{R}}_{x,i} \succeq \sum_{j=1}^{M} \bar{\boldsymbol{W}}_{j,i}$, for any vector $\boldsymbol{v}$, we can write

$$\begin{aligned}&\boldsymbol{v}^H(\hat{\boldsymbol{W}}_{j,i} - \bar{\boldsymbol{W}}_{j,i}) \\ &= \boldsymbol{v}^H\hat{\boldsymbol{W}}_{j,i}\boldsymbol{v} - (\boldsymbol{h}_{j,i}^H\hat{\boldsymbol{W}}_{j,i}\boldsymbol{h}_{j,i})^{-1}|\boldsymbol{v}^H\hat{\boldsymbol{W}}_{j,i}\boldsymbol{h}_{j,i}|^2. \end{aligned} \tag{40}$$

By using the Cauchy-Schwarz inequality, we have

$$\begin{aligned}|\boldsymbol{v}^H\hat{\boldsymbol{W}}_{j,i}\boldsymbol{h}_{j,i}|^2 &= |\boldsymbol{v}^H\hat{\boldsymbol{w}}_{j,i}\hat{\boldsymbol{w}}_{j,i}^H\boldsymbol{v}|^2 \\ &\leq |\boldsymbol{v}^H\hat{\boldsymbol{w}}_{j,i}^H|^2|\boldsymbol{h}_{j,i}^H\hat{\boldsymbol{w}}_{j,i}^H|^2 \\ &= (\boldsymbol{v}^H\hat{\boldsymbol{W}}_{j,i}\boldsymbol{v})(\boldsymbol{h}_{j,i}^H\hat{\boldsymbol{W}}_{j,i}\boldsymbol{h}_{j,i}). \end{aligned} \tag{41}$$

Consequently,

$$\boldsymbol{v}^H(\hat{\boldsymbol{W}}_{j,i} - \bar{\boldsymbol{W}}_{j,i}) \geq 0, \forall j. \tag{42}$$

Hence, $\hat{\boldsymbol{W}}_{j,i} - \bar{\boldsymbol{W}}_{j,i} \succeq 0$. Finally,

$$\begin{aligned}\bar{\boldsymbol{R}}_{x,i} - \sum_{j=1}^{M}\bar{\boldsymbol{W}}_{j,i} &= \hat{\boldsymbol{R}}_{x,i} - \sum_{j=1}^{M}\hat{\boldsymbol{W}}_{j,i} \\ &\quad + \sum_{j=1}^{M}\hat{\boldsymbol{W}}_{j,i} - \bar{\boldsymbol{W}}_{j,i} \succeq 0, \end{aligned} \tag{43}$$

which concludes the proof.

REFERENCES

[1] R. M. Mealey, "A method for calculating error probabilities in a radar communication system," *IEEE Transactions on Space Electronics and Telemetry*, vol. 9, no. 2, pp. 37–42, 1963.

[2] T. Huang, N. Shlezinger, X. Xu, Y. Liu, and Y. C. Eldar, "Majorcom: A dual-function radar communication system using index modulation," *IEEE transactions on signal processing*, vol. 68, pp. 3423–3438, 2020.

[3] C. Sturm and W. Wiesbeck, "Waveform design and signal processing aspects for fusion of wireless communications and radar sensing," *Proceedings of the IEEE*, vol. 99, no. 7, pp. 1236–1259, 2011.

[4] P. Kumari, J. Choi, N. González-Prelcic, and R. W. Heath, "Ieee 802.11 ad-based radar: An approach to joint vehicular communication-radar system," *IEEE Transactions on Vehicular Technology*, vol. 67, no. 4, pp. 3012–3027, 2017.

[5] F. Liu, C. Masouros, A. Li, T. Ratnarajah, and J. Zhou, "Mimo radar and cellular coexistence: A power-efficient approach enabled by interference exploitation," *IEEE Transactions on Signal Processing*, vol. 66, no. 14, pp. 3681–3695, 2018.

[6] Z. Cheng, B. Liao, S. Shi, Z. He, and J. Li, "Co-design for overlaid mimo radar and downlink miso communication systems via cramér–rao bound minimization," *IEEE Transactions on Signal Processing*, vol. 67, no. 24, pp. 6227–6240, 2019.

[7] X. Liu, T. Huang, N. Shlezinger, Y. Liu, J. Zhou, and Y. C. Eldar, "Joint transmit beamforming for multiuser mimo communications and mimo radar," *IEEE Transactions on Signal Processing*, vol. 68, pp. 3929–3944, 2020.

[8] I. Valiulahi, C. Masouros, A. Salem, and F. Liu, "Antenna selection for energy-efficient dual-functional radar-communication systems," *IEEE Wireless Communications Letters*, 2022.

[9] F. Liu, Y. Cui, C. Masouros, J. Xu, T. X. Han, Y. C. Eldar, and S. Buzzi, "Integrated sensing and communications: Towards dual-functional wireless networks for 6g and beyond," *IEEE Journal on Selected Areas in Communications*, 2022.

[10] A. Hassanien, M. G. Amin, Y. D. Zhang, and F. Ahmad, "Dual-function radar-communications: Information embedding using sidelobe control and waveform diversity," *IEEE Transactions on Signal Processing*, vol. 64, no. 8, pp. 2168–2181, 2015.

[11] F. Liu, L. Zhou, C. Masouros, A. Li, W. Luo, and A. Petropulu, "Toward dual-functional radar-communication systems: Optimal waveform design," *IEEE Transactions on Signal Processing*, vol. 66, no. 16, pp. 4264–4279, 2018.

[12] F. Liu, Y.-F. Liu, A. Li, C. Masouros, and Y. C. Eldar, "Cramér-rao bound optimization for joint radar-communication beamforming," *IEEE Transactions on Signal Processing*, vol. 70, pp. 240–253, 2021.

[13] A. R. Chiriyath, B. Paul, G. M. Jacyna, and D. W. Bliss, "Inner bounds on performance of radar and communications co-existence," *IEEE Transactions on Signal Processing*, vol. 64, no. 2, pp. 464–474, 2015.

[14] J. Ma, S. Zhang, H. Li, F. Gao, and S. Jin, "Sparse bayesian learning for the time-varying massive mimo channels: Acquisition and tracking," *IEEE Transactions on Communications*, vol. 67, no. 3, pp. 1925–1938, 2018.

[15] A. F. Molisch and M. Z. Win, "Mimo systems with antenna selection," *IEEE microwave magazine*, vol. 5, no. 1, pp. 46–56, 2004.

[16] Z. Wang, K. Han, X. Shen, W. Yuan, and F. Liu, "Achieving the performance bounds for sensing and communications in perceptive networks: Optimal bandwidth allocation," *IEEE Wireless Communications Letters*, vol. 11, no. 9, pp. 1835–1839, 2022.

[17] E. Vlachos and J. Thompson, "Energy-efficiency maximization of hybrid massive mimo precoding with random-resolution dacs via rf selection," *IEEE Transactions on Wireless Communications*, vol. 20, no. 2, pp. 1093–1104, 2020.

[18] A. Li, C. Masouros, F. Liu, and A. L. Swindlehurst, "Massive mimo 1-bit dac transmission: A low-complexity symbol scaling approach," *IEEE Transactions on Wireless Communications*, vol. 17, no. 11, pp. 7559–7575, 2018.

[19] O. Mehanna, N. D. Sidiropoulos, and G. B. Giannakis, "Joint multicast beamforming and antenna selection," *IEEE Transactions on Signal Processing*, vol. 61, no. 10, pp. 2660–2674, 2013.

[20] J. Yang and S. Ulukus, "Optimal packet scheduling in a multiple access channel with energy harvesting transmitters," *Journal of Communications and Networks*, vol. 14, no. 2, pp. 140–150, 2012.

[21] A. A. Nasir, X. Zhou, S. Durrani, and R. A. Kennedy, "Relaying protocols for wireless energy harvesting and information processing," *IEEE Transactions on Wireless Communications*, vol. 12, no. 7, pp. 3622–3636, 2013.

[22] J. Yang, O. Ozel, and S. Ulukus, "Broadcasting with an energy harvesting rechargeable transmitter," *IEEE Transactions on Wireless Communications*, vol. 11, no. 2, pp. 571–583, 2011.

[23] K. Tutuncuoglu and A. Yener, "Optimum transmission policies for battery limited energy harvesting nodes," *IEEE Transactions on Wireless Communications*, vol. 11, no. 3, pp. 1180–1189, 2012.

[24] D. W. K. Ng, E. S. Lo, and R. Schober, "Energy-efficient resource allocation in ofdma systems with hybrid energy harvesting base station," *IEEE Transactions on Wireless Communications*, vol. 12, no. 7, pp. 3412–3427, 2013.

[25] Z. Zhou, H. Yu, S. Mumtaz, S. Al-Rubaye, A. Tsourdos, and R. Q. Hu, "Power control optimization for large-scale multi-antenna systems," *IEEE Transactions on Wireless Communications*, vol. 19, no. 11, pp. 7339–7352, 2020.

[26] J. Li, L. Xu, P. Stoica, K. W. Forsythe, and D. W. Bliss, "Range compression and waveform optimization for mimo radar: a cramer–rao bound based study," *IEEE Transactions on Signal Processing*, vol. 56, no. 1, pp. 218–232, 2007.

[27] G. Cui, H. Li, and M. Rangaswamy, "Mimo radar waveform design with constant modulus and similarity constraints," *IEEE Transactions on signal processing*, vol. 62, no. 2, pp. 343–353, 2013.

[28] G. Cui, X. Yu, V. Carotenuto, and L. Kong, "Space-time transmit code and receive filter design for colocated mimo radar," *IEEE Transactions on Signal Processing*, vol. 65, no. 5, pp. 1116–1129, 2016.

[29] S. Herbert, J. R. Hopgood, and B. Mulgrew, "Computationally simple mmse (a-optimal) adaptive beam-pattern design for mimo active sensing systems via a linear-gaussian approximation," *IEEE Transactions on Signal Processing*, vol. 66, no. 18, pp. 4935–4945, 2018.

[30] B. Tang, J. Tang, and Y. Peng, "Waveform optimization for mimo radar in colored noise: further results for estimation-oriented criteria," *IEEE Transactions on Signal Processing*, vol. 60, no. 3, pp. 1517–1522, 2011.

[31] M. R. Bell, "Information theory and radar waveform design," *IEEE Transactions on Information Theory*, vol. 39, no. 5, pp. 1578–1597, 1993.

[32] Y. Yang and R. S. Blum, "Mimo radar waveform design based on mutual information and minimum mean-square error estimation," *IEEE Transactions on Aerospace and Electronic Systems*, vol. 43, no. 1, pp. 330–343, 2007.

[33] A. De Maio and M. Lops, "Design principles of mimo radar detectors," *IEEE transactions on Aerospace and Electronic Systems*, vol. 43, no. 3, pp. 886–898, 2007.

[34] B. Tang and J. Li, "Spectrally constrained mimo radar waveform design based on mutual information," *IEEE Transactions on Signal Processing*, vol. 67, no. 3, pp. 821–834, 2018.

[35] A. Goldsmith, *Wireless communications*. Cambridge university press, 2005.

[36] T. M. Cover, "Thomas. elements of information theory," *Wiley Series in Telecommunications*, 1991.

[37] S. Boyd and L. Vandenberghe, *Convex optimization*. Cambridge university press, 2004.

[38] M. Grant, S. Boyd, and Y. Ye, "cvx users' guide," *online: http://www. stanford. edu/˜ boyd/software. html*, 2009.

[39] B. Recht, M. Fazel, and P. A. Parrilo, "Guaranteed minimum-rank solutions of linear matrix equations via nuclear norm minimization," *SIAM review*, vol. 52, no. 3, pp. 471–501, 2010.

[40] M. Grant, S. Boyd, and Y. Ye, "Cvx: Matlab software for disciplined convex programming," 2008.

[41] K. T. Phan, S. A. Vorobyov, N. D. Sidiropoulos, and C. Tellambura, "Spectrum sharing in wireless networks via qos-aware secondary multicast beamforming," *IEEE Transactions on signal processing*, vol. 57, no. 6, pp. 2323–2335, 2009.

[42] B. Tang, M. M. Naghsh, and J. Tang, "Relative entropy-based waveform design for mimo radar detection in the presence of clutter and interference," *IEEE transactions on signal processing*, vol. 63, no. 14, pp. 3783–3796, 2015.

[43] F. Liu and C. Masouros, "Hybrid beamforming with sub-arrayed mimo radar: Enabling joint sensing and communication at mmwave band," in *ICASSP 2019-2019 IEEE International Conference on Acoustics, Speech and Signal Processing (ICASSP)*, pp. 7770–7774, IEEE, 2019.

[44] A. Kaushik, C. Masouros, and F. Liu, "Hardware efficient joint radar-communications with hybrid precoding and rf chain optimization," in *ICC 2021-IEEE International Conference on Communications*, pp. 1–6, IEEE, 2021.

[45] L. You, X. Qiang, C. G. Tsinos, F. Liu, W. Wang, X. Gao, and B. Ottersten, "Beam squint-aware integrated sensing and communications for hybrid massive mimo leo satellite systems," *arXiv preprint arXiv:2203.00235*, 2022.

[46] E. Chen and M. Tao, "Admm-based fast algorithm for multi-group multicast beamforming in large-scale wireless systems," *IEEE Transactions on Communications*, vol. 65, no. 6, pp. 2685–2698, 2017.